Possible identifications of newly observed magnetar quasi-periodic oscillations as crustal shear modes

Hajime Sotani[1], Kei Iida[2], Kazuhiro Oyamatsu[3]

[1] *Division of Theoretical Astronomy, National Astronomical Observatory of Japan, 2-21-1 Osawa, Mitaka, Tokyo 181-8588, Japan*

[2] *Department of Natural Science, Kochi University, 2-5-1 Akebono-cho, Kochi 780-8520, Japan*

[3] *Department of Human Informatics, Aichi Shukutoku University, 2-9 Katahira, Nagakute, Aichi 480-1197, Japan*

Abstract

Quasi-periodic oscillations (QPOs) discovered in soft-gamma repeaters (SGRs) are expected to help us to study the properties of matter in neutron stars. In earlier investigations, we identified the QPOs of frequencies below ~ 100 Hz observed in giant flares of SGR 1806−20 and SGR 1900+14 as the crustal torsional oscillations. For this purpose, we calculated the frequencies of the fundamental torsional oscillations with various angular indices ℓ, by changing the stellar mass and radius. In this work, we try to explain the additional QPO frequencies recently reported by Huppenkothen et al. [1, 2] within the same framework as before except that we newly take into account the effect of electron screening, which acts to decrease the frequencies by a small amount. Those QPOs were discovered in two different SGRs, i.e., SGR 1806−20 and SGR J1550−5418. Then, we find that the newly observed QPO frequency in SGR 1806−20 can be still identified as one of the frequencies of the fundamental torsional oscillations, while those in SGR J1550−5418 can also be explained in terms of the torsional oscillations although the relevant angular indices are difficult to identify.

Keywords: neutron stars, equation of state, oscillations

Email address: hajime.sotani@nao.ac.jp (Hajime Sotani[1])

1. Introduction

Neutron stars, which are stellar remnants of the core collapse of massive stars, give us one of the best opportunities to investigate the physics under extreme conditions. This is partly because the density of matter inside the star can become significantly larger than normal nuclear density, partly because some neutron stars are strongly magnetized while others are rapidly rotating, and partly because the gravitational fields around neutron stars are strong enough for effects of general relativity to manifest themselves. Astronomical phenomena associated with neutron stars could leave imprint of the physics under such extreme conditions. The asteroseismology is a powerful technique to reveal the interiors of neutron stars via their oscillation spectra, as in the case of the seismology in the Earth and the helioseismology in the Sun. In fact, through detection of the frequencies of neutron star oscillations, it might be possible to deduce neutron star masses and radii, the equation of state (EOS) of matter in the star, and so on (e.g., [3, 4, 5, 6, 7]). Gravitational waves, if detected, could be one of the most promising sources that provide the oscillation spectra of neutron stars.

Alternatively, it is expected that observational evidences for neutron star oscillations have already been given as the quasi periodic oscillations (QPOs) observed from soft gamma repeaters (SGRs) in the afterglow of the giant flares. Up to now, at least three giant flares were observed, and various QPO frequencies were found in two of them, which radiated from SGR 1806−20 and SGR 1900+14 [8, 9, 10]. Since SGRs are considered to be magnetars, which are strongly magnetized neutron stars, the observed QPOs are expected to be strongly associated with the neutron star oscillations. There are many attempts to explain these QPOs theoretically, which are based on shear torsional oscillations in the crustal region of a neutron star and/or magnetic oscillations throughout the star (e.g., [11, 12, 13, 14, 15, 16, 17]). Subsequently, analyses of elastic-magnetic oscillations in magnetars reveal that, depending on the magnetic field strength, the oscillations near the star's surface are excited basically by either crustal torsional oscillations or magnetic oscillations [18, 19]. According to observational estimates of the surface magnetic field strength of the SGRs from which the giant flares radiate [20, 21], the magnetic field in the star can give rise to a restoring force, whose strength is comparable to that induced by the crustal shear modulus, and hence shear torsional oscillations and magnetic oscillations are almost indistinguishable. However, given that the highest magnetic fields are more

or less localized, e.g., in a toroidal form, it is reasonable to start with the assumption that the QPOs observed in SGRs are identified as the crustal torsional oscillations. Then, such an identification could tell us information about the properties of the crust, particularly the EOS [22, 23, 24].

One of the most important parameters characterizing the EOS of neutron-rich matter in the crust is the density dependence of the nuclear symmetry energy, L, which is strongly associated with the thickness of the region where nuclei exist as non-uniform nuclear structures [25, 26, 27]. The constraint on L can be given via the terrestrial nuclear experiments [28], but it is still difficult to obtain a severe constraint. On the other hand, we developed a way of constraining L through the identification of the QPOs observed in SGRs as the crustal torsional oscillations [29, 30, 31] as well as through possible simultaneous mass and radius measurements of low-mass neutron stars [32]. This is a constraint from nuclear matter at extremely large neutron excess, in contrast with the case of the terrestrial nuclear experiments associated with nuclear matter at relatively small neutron excess.

Recently, new QPO frequencies in SGR J1550−5418 and SGR 1806−20 have been reported. In SGR J1550−5418, the QPO frequencies of 93 and 127 Hz have been discovered from a storm of 286 bursts [1]. In addition, the QPO frequency of 57 Hz has been discovered in the shorter and less energetic recurrent 30 bursts radiating from SGR 1806−20 [2]. Since the QPO of frequency 57 Hz comes from the same SGR as that from which the giant flare was detected, it is important to make sure that this new QPO frequency can be explained within the framework that reproduces the low-lying QPO frequencies found in the giant flare. Meanwhile, although SGR J1550−5418 adds to a list of the SGRs that have the QPOs detected, unfortunately the observed QPO frequencies are limited and not low enough to clearly identify the corresponding angular indices. Thus, we here systematically examine how valid the crustal torsional oscillations are to explain the QPO frequencies observed in the SGRs. In order to calculate the frequencies of the crustal torsional oscillations, we adopt the shear modulus that allows for the effect of electron screening on nuclei in the crust [33]. Additionally, as the effect of neutron superfluidity on the enthalpy density of matter in the inner crust, we adopt the results for the superfluid density given by Chamel [34], as in Refs. [30, 31]. We adopt the geometric unit of $c = G = 1$ in this paper, where c and G denote the speed of light and the gravitational constant, respectively.

2. Crust configuration and EOS parameters

In the vicinity of the saturation point of symmetric nuclear matter at zero temperature, the bulk energy of nuclear matter per nucleon w can be generally expressed as a function of baryon number density $n_{\rm b}$ and neutron excess α, as in Ref. [35]:

$$w = w_0 + \frac{K_0}{18n_0^2}(n_{\rm b} - n_0)^2 + \left[S_0 + \frac{L}{3n_0}(n_{\rm b} - n_0)\right]\alpha^2, \tag{1}$$

where w_0, n_0, and K_0 are the saturation energy, saturation density, and incompressibility of symmetric nuclear matter ($\alpha = 0$). In addition, S_0 and L are associated with the density dependent symmetry energy $S(n_{\rm b})$ as $S_0 \equiv S(n_0)$ and $L \equiv 3n_0(dS/dn_{\rm b})_{n_{\rm b}=n_0}$. Note that only w_0, n_0, and S_0 among the five parameters are well constrained from empirical data for masses and radii of stable nuclei [36].

In describing matter in the crust of a neutron star, we follow the derivation by two of the authors (K.O. and K.I.), which is based on a phenomenological approach [27]. Hereafter, we refer to the resultant phenomenological EOS of matter in the crust as OI-EOS. The OI-EOS is constructed as follows. First, various models for the bulk energy $w(n_{\rm b}, \alpha)$ of nuclear matter are made in such a way as to reproduce Eq. (1) in the limit of $n_{\rm b} \to 0$ and $\alpha \to 0$. Then, within a simplified version of the extended Thomas-Fermi theory, the density profile of stable nuclei was obtained for each model for w. Finally, the optimal values of w_0, n_0, and S_0 were determined so that the charge number, mass excess, and charge radius that can be calculated from the density profile obtained for given $y \equiv -K_0S_0/(3n_0L)$ and K_0 should fit well to the experimental data [36]. After that, in order to obtain the equilibrium nuclear shape and size as well as the crust EOS for various sets of y and K_0, we generalized the Thomas-Fermi model by adding dripped neutrons, a neutralizing uniform background of electrons, and the lattice energy within a Wigner-Seitz approximation [27]. In the present work, as in Refs. [27, 29, 30, 31], we consider the parameters L, K_0, and y in the range of $0 < L < 160$ MeV, $180 \leq K_0 \leq 360$ MeV, and $y < -200$ MeV fm^3, which can not only reproduce the mass and radius data for stable nuclei equally well, but also effectively cover even extreme cases [36]. The eleven parameter sets adopted in this work are the same as in Table 1 in Ref. [31].

For given mass M and radius R of a nonrotating neutron star, the crust configuration can be constructed by integrating the Tolman-Oppenheimer-

Volkoff equations with the above-mentioned crust EOS from the star's surface inward up to the basis of the crust [37, 29, 30, 31]. This construction effectively avoids uncertainties in the core EOS. In this work, we particularly consider typical neutron star models with M and R in the range of $1.4 \leq M/M_\odot \leq 1.8$ and 10 km $\leq R \leq 14$ km.

One of the crucial properties that govern the shear oscillations is the elasticity, which is characterized by the shear modulus μ. The shear modulus in the crust is mainly determined by the lattice energy due to the Coulomb interaction, which is approximately given as

$$\mu = 0.1194 \times \frac{n_i (Ze)^2}{a}, \tag{2}$$

where n_i, Z, and $a = (3/4\pi n_i)^{1/3}$ are the ion number density, the nuclear charge number, and the radius of a Wigner-Seitz cell, respectively [38]. This formula is derived in the limit of zero temperature from Monte Carlo calculations averaged over all directions on the assumption that the nuclei are point particles forming the body-center cubic lattice [39].

On the other hand, Kobyakov and Pethick proposed the modification of the shear modulus, where the effect of electron screening is taken into account [33]. The modified shear modulus can be expressed as

$$\mu = 0.1194 \left(1 - 0.010 Z^{2/3}\right) \frac{n_i (Ze)^2}{a}, \tag{3}$$

where the term of $Z^{2/3}$ represents the effect of electron screening. That is, the shear modulus decreases due to such additional effect, which in turn leads to reduction of the frequencies of torsional oscillations [40][1]. Since the charge number Z also depends on L, however, it is still unclear how the reduction of the frequencies of torsional oscillations due to the effect of electron screening depends on L. At subnuclear densities, Z tends to decrease with L, because the smaller symmetry energy, corresponding to larger L, helps more protons to change into neutrons. In fact, Z decreases with L for the OI-EOS adopted in the present work, as shown in Fig. 1. Consequently, one expects that the frequencies of torsional oscillations by using the modified shear modulus [Eq.

[1]The electron screening acts to change the toroidal oscillation frequencies also via modifications of the enthalpy density and the crustal structure, but such change is negligibly small.

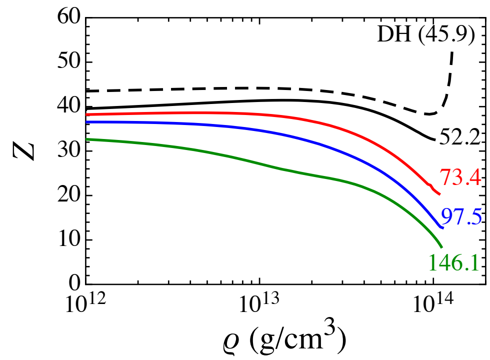

Figure 1: (Color online) Nuclear charge number, Z, plotted as a function of the energy density, ρ, for the OI-EOS with various values of L. The labels on the solid lines denote the values of L; L = 52.2, 73.4, 97.5, and 146.1 MeV correspond to the OI-EOS with (y, K_0)=(-220 MeV fm^3, 180 MeV), (-220 MeV fm^3, 230 MeV), (-220 MeV fm^3, 280 MeV), and (-220 MeV fm^3, 360 MeV). For reference, the result from the EOS proposed by Douchin & Haensel [41] is also shown with the broken line, where the corresponding value of L is 45.9 MeV.

(3)] differs little from those by using the original shear modulus [Eq. (2)], if L is sufficiently large. Even so, we will examine the torsional oscillations with the modified shear modulus [Eq. (3)] in this work.

3. Crustal torsional oscillations in neutron stars

We proceed to calculate the fundamental frequencies of the torsional oscillations that are excited in the crust of a nonrotating neutron star of mass M and radius R as constructed from the crust EOS of a given set of L and K_0 in the previous section. In particular, we adopt the relativistic Cowling approximation to calculate the frequencies. That is, we neglect the metric perturbations and keep them zero during the oscillations. This is presumably a good approximation for considering the torsional oscillations, because they are axial parity oscillations, which do not involve the density perturbations. The perturbation equation for the torsional oscillations can be obtained from the linearized relativistic equation of motion [42]. Then, imposing the appropriate boundary conditions at the top and bottom of the crust, the problem to solve reduces to the eigenvalue problem, where the eigenvalues correspond to the eigen-frequencies of the torsional oscillations. The perturbation equation and the boundary conditions are explicitly described in Ref. [31]; pasta

nuclei, if present, are assumed to have zero shear modulus.

Additionally, the effect of dripped neutrons should be taken into account for the calculation of the frequencies of the torsional oscillations. In fact, neutrons are generally considered to drip out of nuclei when the density becomes higher than $\sim 4 \times 10^{11}$ g/cm^3, and some of them behave as a superfluid. Unfortunately, it is still unclear how many dripped neutrons behave as such, but most of them can move together with the nuclei because of the entrainment effects [34]. In fact, according to the results from the band calculations in Ref. [34], only of the order of $10 - 30$ % of the dripped neutrons can participate in superfluidity at $n_{\rm b} \sim 0.01 - 0.4 n_0$. Through the enthalpy density, the frequencies of the torsional oscillations depends strongly on this ratio [30]; we adopt the results by Chamel [34] in the present work. Then, we calculate the frequencies based on the prescription how to build the effect of superfluidity into the perturbation equations shown in Ref. [31].

First, to see the dependence of the frequencies on the parameters that characterize the crust EOS, L and K_0, we calculate the frequencies of the fundamental torsional oscillations with $\ell = 2$ for the stellar models with $M = 1.4 M_\odot$ and $R = 12$ km. The calculated frequencies are plotted as a function of L for various values of K_0 in Fig. 2. Note that the shear torsional oscillations are often referred to as t-modes, which are labelled as ${}_n t_\ell$ with the angular index ℓ and the number n of radial nodes in the eigenfunction. From this figure, one can observe that the frequency ${}_0 t_2$ is almost independent of the incompressibility K_0, while depending strongly on L. This tendency has been already shown in the case in which ${}_n t_\ell$ is calculated from the shear modulus [Eq. (2)] in Ref. [30], but still holds in the case of the modified shear modulus [Eq. (3)]. Since we confirm that this is true for different stellar models within $1.4 \leq M/M_\odot \leq 1.8$ and 10 km $\leq R \leq$ 14 km, ${}_0 t_2$ can be approximately expressed as

$$ {}_0 t_2 = c_2^{(0)} - c_2^{(1)} L + c_2^{(2)} L^2, \tag{4}$$

where $c_2^{(0)}$, $c_2^{(1)}$, and $c_2^{(2)}$ denote positive coefficients that depend on the stellar models. In practice, this fitting formula agrees well with the calculated frequencies for various sets of the EOS parameters within the accuracy of a few per cent, as shown in Table 1.

In a similar way, we find that the frequencies ${}_0 t_\ell$ for $\ell > 2$ are almost independent of K_0 and can be approximately expressed as a function of L via

$$ {}_0 t_\ell = c_\ell^{(0)} - c_\ell^{(1)} L + c_\ell^{(2)} L^2, \tag{5}$$

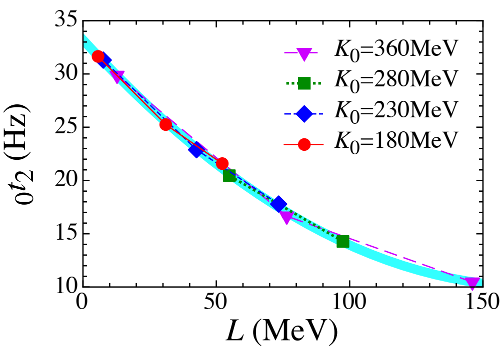

Figure 2: (Color online) The frequency of the fundamental torsional oscillations with $\ell = 2$, ${}_0t_2$, plotted as a function of L for the stellar models with $M = 1.4M_\odot$ and $R = 12$ km. The thick solid line denotes the fitting formula [Eq. (4)].

Table 1: The numerically calculated values of the frequency of the $\ell = 2$ fundamental torsional oscillations, ${}_0t_2^{(c)}$, and the values obtained from Eq. (4), ${}_0t_2^{(e)}$, for the stellar models of $M = 1.4M_\odot$ and $R = 12$ km. The relative errors determined by $({}_0t_2^{(c)} - {}_0t_2^{(e)})/{}_0t_2^{(c)}$ are also tabulated.

y (MeV fm^3)	K_0 (MeV)	L (MeV)	${}_0t_2^{(c)}$ (Hz)	${}_0t_2^{(e)}$ (Hz)	relative error (%)
−220	180	52.2	21.59	21.12	2.14
−220	230	73.4	17.79	17.49	1.71
−220	280	97.5	14.28	14.21	0.43
−220	360	146.1	10.46	10.47	−0.15
−350	180	31.0	25.25	25.49	−0.98
−350	230	42.6	22.89	23.02	−0.60
−350	280	54.9	20.45	20.63	−0.86
−350	360	76.4	16.65	17.02	−2.21
−1800	180	5.7	31.65	31.68	−0.12
−1800	230	7.6	31.30	31.17	0.41
−1800	360	12.8	29.87	29.84	0.08

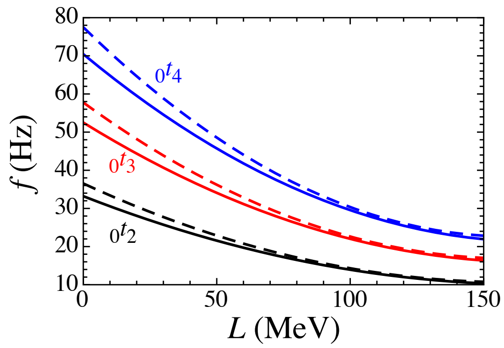

Figure 3: (Color online) The frequencies of the fundamental torsional oscillations with $\ell = 2$, 3, and 4, plotted as a function of L for the stellar models with $M = 1.4M_\odot$ and $R = 12$ km. The broken lines correspond to the frequencies calculated from the shear modulus [Eq. (2)], while the solid lines correspond to those from Eq. (3).

where $c_\ell^{(0)}$, $c_\ell^{(1)}$, and $c_\ell^{(2)}$ are adjustable parameters.

In Fig. 3, we show the comparison between the frequencies calculated from the shear modulus [Eq. (2)] and those from the modified shear modulus [Eq. (3)] for the stellar models with $M = 1.4M_\odot$ and $R = 12$ km. As discussed in the previous section, the deviations in ${}_0t_\ell$ due to the effect of electron screening increase with decreasing L, but almost vanish for large L.

4. Comparison with the QPO frequencies

Let us now compare the calculated frequencies ${}_0t_\ell$ with the QPO frequencies observed in SGRs. The identification of the QPO frequencies observed in SGR 1806−20 as the frequencies ${}_0t_\ell$ is more difficult than that in SGR 1900+14, because not only many QPO frequencies are discovered in SGR 1806−20 but also the interval between the observed QPO frequencies 26 and 30 Hz is remarkably small [14]. Nevertheless, as shown in Refs. [30, 31], the QPO frequencies 18, 26, 30, and 92.5 Hz observed in SGR 1806−20 can be explained well in terms of the fundamental torsional oscillations with $\ell = 3, 4, 5$, and 15, where the frequencies of the torsional oscillations are calculated from the original shear modulus [Eq. (2)]. Here, we re-calculate the frequencies from the modified shear modulus [Eq. (3)]. Then, we find that the same correspondence as in Refs. [30, 31] is still intact, as shown in Fig. 4 for the stellar models with $M = 1.4M_\odot$ and $R = 12$ km. We remark

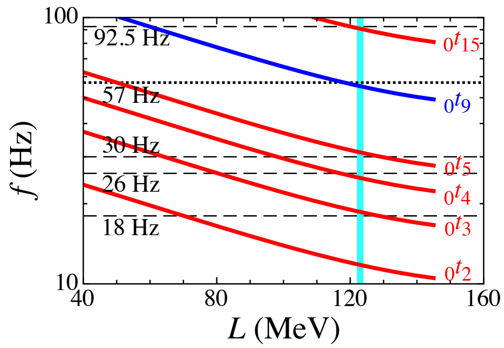

Figure 4: (Color online) Correspondence between the QPO frequencies observed in SGR 1806−20 and the calculated frequencies of the fundamental torsional oscillations for the stellar models with $M = 1.4M_\odot$ and $R = 12$ km. The horizontal broken lines denote the QPO frequencies originally reported by Israel et al. [8], Strohmayer & Watts [10], while the horizontal dotted line denotes the new QPO frequency discovered by Huppenkothen et al. [2]. The vertical line denotes the value of $L = 123$ MeV, with which the observed QPO frequencies agree best with the calculated frequencies of the crustal torsional oscillations.

that the reproduction of the QPO frequencies by the crustal torsional oscillations is equally good. Moreover, we also include the new QPO frequency 57 Hz reported by [2] in this figure, and we find that this additional QPO frequency can be identified as the $\ell = 9$ fundamental torsional oscillations. As can be seen from Fig. 4, the most suitable value of L to adjust the crustal torsional oscillations to the five observed QPO frequencies is $L = 123$ MeV, with which the frequencies obtained from Eq. (5) and their relative errors from the observed QPO frequencies are shown in Table 2. Since not only the QPO frequencies discovered from the giant flare but also that observed from the different event in the same object, SGR 1806−20, can be explained in the same framework, we conclude that the torsional oscillations are still promising as the origin of the QPOs from SGRs.

The same identification between the QPO frequencies observed in SGR 1806−20 and the crustal torsional oscillations is also possible for different stellar models. In Fig. 5, we plot the optimal values of L to explain the observed QPO frequencies for various stellar models within $1.4 \leq M/M_\odot \leq 1.8$ and $10\ \text{km} \leq R \leq 14$ km.

Unlike SGR 1806−20, the observed QPO frequencies in SGR 1900+14 can be simply explained in terms of the crustal torsional oscillations. As in Ref. [30], we find that the observed QPOs of frequencies 28, 54, and 84

Table 2: The QPO frequencies observed in SGR 1806−20, the corresponding angular indices and frequencies of the fundamental torsional oscillations, the latter of which are obtained from Eq. (5) by substituting the optimal value into L for $M = 1.4M_\odot$, and $R = 12$ km, and their relative errors from the observed QPO frequencies.

QPO frequency (Hz)	ℓ	${}_0t_\ell^{(e)}$ (Hz)	relative error (%)
18	3	18.62	−3.44
26	4	24.98	3.92
30	5	31.15	−3.85
57	9	55.22	3.13
92.5	15	90.76	1.88

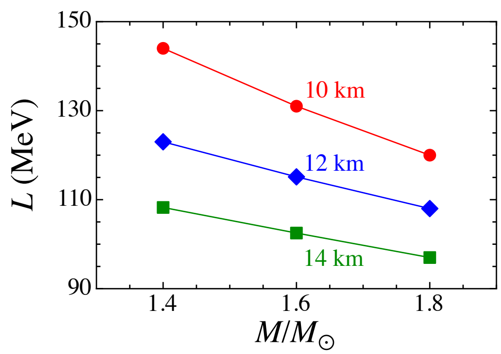

Figure 5: (Color online) The optimal values of L to explain the QPO frequencies observed in SGR 1806−20, as in Fig. 4, for various stellar models. In the figure, the circles, diamonds, and squares correspond to the results for the stellar models with $R = 10$, 12, and 14 km.

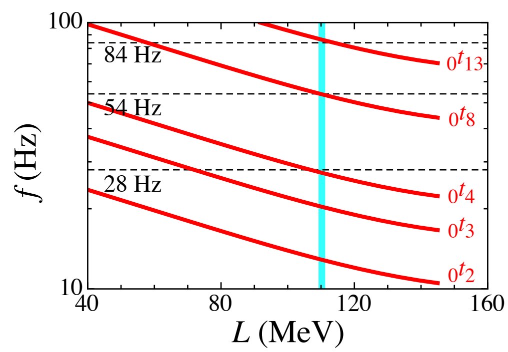

Figure 6: (Color online) Same as Fig. 4, but for the QPO frequencies observed in SGR 1900+14.

Table 3: Same as Table 2, but for the QPO frequencies observed in SGR 1900+14.

QPO frequency (Hz)	ℓ	${}_0t_\ell^{(e)}$ (Hz)	relative error (%)
28	4	27.29	2.55
54	8	53.80	0.36
84	13	86.26	−2.69

Hz can be identified as $\ell = 4, 8$, and 13 even for the calculations from the modified shear modulus (3). In Fig. 6, we show such an identification for the stellar models with $M = 1.4M_\odot$ and $R = 12$ km, together with the optimal value of L to explain the observed QPO frequencies, i.e., $L = 110$ MeV. We also show the comparison between the observed QPO and calculated frequencies for the stellar models with $M = 1.4M_\odot$ and $R = 12$ km in Table 3. Additionally, we find that the observed QPO frequencies can be explained by the same identification even for various stellar models, where the corresponding optimal value of L to explain the observed QPO frequencies in SGR 1900+14 is shifted as shown in Fig. 7.

Although the value of L still depends on many uncertainties, it is reasonable to try to simultaneously explain the QPO frequencies observed in SGR 1806−20 and SGR 1900+14 for a specific value of L. As shown in Fig. 8, therefore, we can constrain L as $97 \le L \le 127$ MeV by assuming that the central objects in SGR 1806−20 and SGR 1900+14 are neutron stars whose mass and radius are in the range of $1.4 \le M/M_\odot \le 1.8$ and 10 km $\le R \le 14$ km. Comparing to the constraint on L obtained in Ref. [31] from the shear modulus [Eq. (2)], the current constraint shifts to lower values by

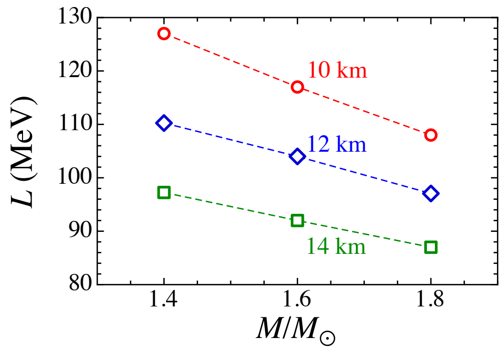

Figure 7: (Color online) Same as Fig. 5, but for the QPO frequencies observed in SGR 1900+14.

about 4 MeV due to the effect of electron screening. We also remark that the obtained constraint is still consistent with that from an X-ray busting neutron star [43].

Furthermore, we proceed to the QPO frequencies observed in SGR J1550−5418, which give us information independent of SGR 1806−20 and SGR 1900+14. Unfortunately, there are only two QPO frequencies observed, 93 and 127 Hz [1]. The observed frequencies, which are relatively high, might arise from the same oscillation mechanism other than the crustal torsional oscillations, but, as we shall see, the crustal torsional oscillations have little difficulty in reproducing the observed QPO frequencies.

In Fig. 9, the frequencies of the fundamental torsional oscillations with $\ell = 11 - 25$ are shown as a function of L for the stellar models with $M = 1.4M_\odot$ and $R = 12$ km, together with the observed QPO frequencies. From this figure, one finds various combinations of ${}_0t_\ell$ that can reproduce the observed QPO frequencies. In practice, if the observed QPO frequencies 93 Hz and 127 Hz are regarded as the frequencies of the fundamental torsional oscillations with ℓ_1 and $\ell_2(>\ell_1)$, one can find that $(\ell_1, \ell_2) = (11, 15), (12, 16), (13, 18), (14, 19), (15, 21), (16, 22), (17, 23)$, and $(18, 25)$ are relevant as shown by the vertical solid lines in Fig. 9, where the corresponding optimal values of L are 81, 90, 101, 109, 121, 130, 139, and 161 MeV, respectively. Additionally, in Table 4, we show the possible combinations of ℓ_1 and ℓ_2, the frequencies of the corresponding torsional oscillations that can be obtained from Eq. (5) by substituting the optimal values into L for $M = 1.4M_\odot$ and $R = 12$ km, and their relative errors from the observed

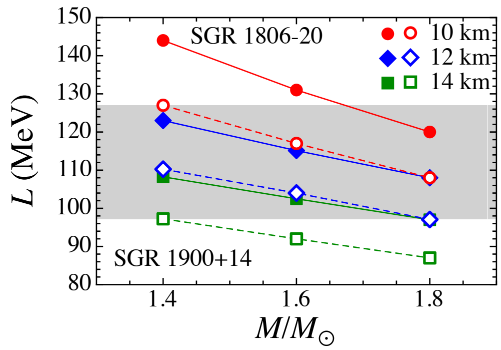

Figure 8: (Color online) The allowed values of L (shaded region) that can simultaneously explain the QPO frequencies observed in SGR 1806−20 and 1900+14, if the corresponding central objects are neutron stars having mass and radius in the range of $1.4 \leq M/M_\odot \leq 1.8$ and 10 km $\leq R \leq$ 14 km.

QPO frequencies. Considering the accuracy of the fitting formula (5) as well as the limited number of the observed QPO frequencies, we have difficulty in judging which combination is in best agreement with the observed QPO frequencies.

Assuming that the central object in SGR J1550−5418 is a neutron star within $1.4 \leq M/M_\odot \leq 1.8$ and 10 km $\leq R \leq$ 14 km, we show in Fig. 10 that several combinations of (ℓ_1, ℓ_2) are consistent with the constraint on L from the QPO frequencies observed in SGR 1806−20 and SGR 1900+14 as described in Fig. 8. As in the case of SGR 1806−20 and SGR 1900+14 shown in Figs. 5 and 7, the upper and lower limits of the constraint on L for each (ℓ_1, ℓ_2) in Fig. 10 are determined by the stellar models with (M, R)=($1.4M_\odot$, 10 km) and ($1.8M_\odot$, 14 km), respectively. From this figure, we find that at least the identification of the QPOs observed in SGR J1550−5418 as the fundamental torsional oscillations with $\ell = 11$ and 15 is not consistent with the constrained region of L from the QPO frequencies observed in SGR 1806−20 and SGR 1900+14. Additional discoveries of the QPO frequencies in SGR J1550−5418 would enable us to tell which of the remaining possibilities is best, which in turn leads to severer constraint on L.

5. Conclusion

In summary, we show that the observed low-lying QPOs, including the new ones from SGR 1806−20 and SGR J1550−5418, can be still identified as

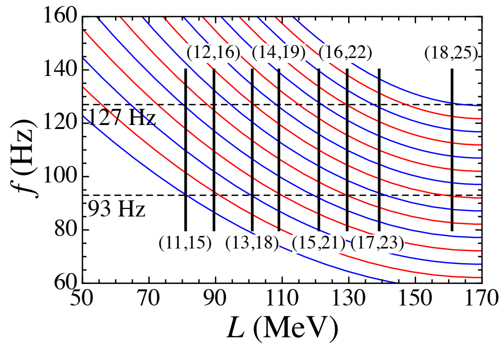

Figure 9: (Color online) The frequencies of the fundamental torsional oscillations with $\ell = 11 - 25$, which are evaluated as a function of L for the stellar models with $M = 1.4M_\odot$ and $R = 12$ km. The horizontal broken lines denote the QPO frequencies observed in SGR J1550−5418. The vertical lines denote various possible correspondences between the QPO frequencies and the frequencies of the fundamental torsional oscillations with the values of ℓ represented by $(*, *)$ in the figure.

Table 4: Same as Table 2, but for the QPO frequencies observed in SGR J1550−5418, where various combinations of ℓ to explain the observed QPO frequencies can be considered.

QPO frequency (Hz)	ℓ	${}_0t_\ell^{(e)}$ (Hz)	relative error (%)
93	11	93.19	−0.21
127	15	126.1	0.73
93	12	94.26	−1.35
127	16	124.8	1.74
93	13	92.66	0.37
127	18	127.4	−0.28
93	14	93.59	−0.63
127	19	126.1	0.70
93	15	91.94	1.14
127	21	127.7	−0.57
93	16	92.91	0.098
127	22	126.8	0.15
93	17	93.77	−0.83
127	23	125.9	0.84
93	18	92.61	0.42
127	25	127.5	−0.40

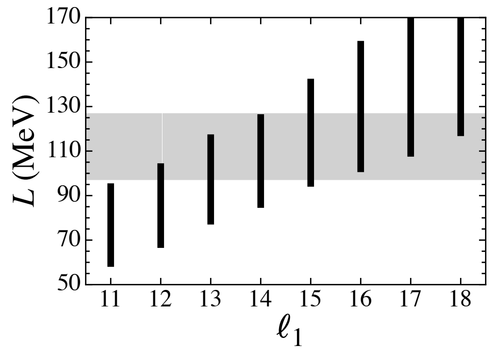

Figure 10: The allowed regions of L to explain the QPO frequencies observed in SGR J1550−5418 in terms of the fundamental torsional oscillations for the stellar models with the mass and radius in the range of $1.4 \leq M/M_\odot \leq 1.8$ and $10\ \text{km} \leq R \leq 14$ km. The horizontal axis ℓ_1 denotes the angular index as which the lower QPO frequency 93 Hz is identified, as shown in Table 4. The shaded region is the constraint on L from the QPO frequencies observed in SGR 1806−20 and SGR 1990+14 as described in Fig. 8. We set the upper limit of the vertical axis at $L = 170$ MeV, above which extrapolations based on Eq. (5) are no longer effective.

the crustal fundamental torsional oscillations with different ℓ's. This result gives a strong indication that the QPOs and the crustal modes are more or less related. However, there remain many problems. To make better estimates of the frequencies of the crustal modes, which are given as a function of the EOS parameter L and the neutron star mass M and radius R in the present work, it is indispensable to take into account effects of magnetic fields on the effective shear modulus. Unfortunately, it would be a tall task given poorly known magnetic structure. Even within the framework of purely elastic shear modes as considered in the present work, how to average the locally anisotropic shear modulus over directions for a polycrystal could modify the effective shear modulus significantly [44]. Also, stability of the bcc structure as assumed here is endangered by fluctuations in the density of dripped neutrons; the resultant change in the lattice structure could affect the effective shear modulus and modifications of the enthalpy density by neutron superfluidity [45]. Note that with all those theoretical uncertainties, one can definitely assign the angular index ℓ to each QPO except the two QPOs observed in SGR J1550−5418; assignment of these two QPOs would be possible only after possible observations of additional low-lying QPOs from the same source.

This work was supported in part by Grants-in-Aid for Scientific Research on Innovative Areas through No. 15H00843 and No. 24105008 provided by MEXT and by Grant-in-Aid for Young Scientists (B) through No. 26800133 provided by JSPS.

References

[1] D. Huppenkothen et al., Astrophys. J. 787 (2014) 128

[2] D. Huppenkothen, L. M. Heil, A. L. Watts, and E. Göğüş, Astrophys. J. 795 (2014) 114

[3] N. Andersson and K. D. Kokkotas, Phys. Rev. Lett. 77 (1996) 4134

[4] H. Sotani, K. Tominaga, and K. I. Maeda, Phys. Rev. D 65 (2001) 024010

[5] H. Sotani and T. Harada, Phys. Rev. D 68 (2003) 024019;
H. Sotani, K. Kohri, and T. Harada, Phys. Rev. D 69 (2004) 084008

[6] H. Sotani, N. Yasutake, T. Maruyama, and T. Tatsumi, Phys. Rev. D 83 (2011) 024014

[7] D. D. Doneva, E. Gaertig, K. D. Kokkotas, and C. Krüger, Phys. Rev. D, 88 (2013) 044052

[8] G. Israel et al., Astrophys. J. 628 (2005) L53

[9] T. E. Strohmayer and A. L. Watts, Astrophys. J. 632 (2005) L111

[10] T. E. Strohmayer and A. L. Watts, Astrophys. J. 653 (2006) 593

[11] Y. Levin, Mon. Not. R. Astron. Soc. 368 (2006) L35;
Y. Levin, Mon. Not. R. Astron. Soc. 377 (2007) 159

[12] U. Lee, Mon. Not. R. Astron. Soc. 374 (2007) 1015

[13] L. Samuelsson and N. Andersson, Mon. Not. R. Astron. Soc. 374 (2007) 256

[14] H. Sotani, K. D. Kokkotas, and N. Stergioulas, Mon. Not. R. Astron. Soc. 375 (2007) 261

[15] H. Sotani, K. D. Kokkotas, and N. Stergioulas, Mon. Not. R. Astron. Soc. 385 (2008) L5

[16] H. Sotani, A. Colaiuda, and K. D. Kokkotas, Mon. Not. R. Astron. Soc. 385 (2008) 2161

[17] H. Sotani and K. D. Kokkotas, Mon. Not. R. Astron. Soc. 395 (2009) 1163

[18] A. Colaiuda and K. D. Kokkotas, Mon. Not. R. Astron. Soc. 414 (2011) 3014

[19] M. Gabler, P. Cerdá-Durán, N. Stergioulas, J. A. Font, and E. Müller, Mon. Not. R. Astron. Soc. 421 (2012) 2054

[20] C. Kouveliotou et al., Nature 393 (1998) L235

[21] K. Hurley et al., Nature 397 (1999) L41

[22] A. W. Steiner and A. L. Watts, Phys. Rev. Lett. 103 (2009) 181101

[23] M. Gearheart, W. G. Newton, J. Hooker, and B. A. Li, Mon. Not. R. Astron. Soc. 418 (2011) 2343

[24] H. Sotani, Mon. Not. R. Astron. Soc. 417 (2011) L70

[25] C. P. Lorenz, D. G. Ravenhall, and C. J. Pethick, Phys. Rev. Lett. 70 (1993) 379

[26] K. Oyamatsu, Nucl. Phys. A 561 (1993) 431

[27] K. Oyamatsu and K. Iida, Phys. Rev. C 75 (2007) 015801

[28] M. B. Tsang et al., Phys. Rev. C 86 (2012) 015803

[29] H. Sotani, K. Nakazato, K. Iida, and K. Oyamatsu, Phys. Rev. Lett. 108 (2012) 201101

[30] H. Sotani, K. Nakazato, K. Iida, and K. Oyamatsu, Mon. Not. R. Astron. Soc. 428 (2013) L21

[31] H. Sotani, K. Nakazato, K. Iida, and K. Oyamatsu, Mon. Not. R. Astron. Soc. 434 (2013) 2060

[32] H. Sotani, K. Iida, K. Oyamatsu, and A. Ohnishi, Prog. Theor. Exp. Phys. 2014 (2014) 051E01

[33] D. Kobyakov and C. J. Pethick, Phys. Rev. C 87 (2013) 055803

[34] N. Chamel, Phys. Rev. C 85 (2012) 035801

[35] J. M. Lattimer, Annu. Rev. Nucl. Part. Sci. 31 (1981) 337

[36] K. Oyamatsu and K. Iida, Prog. Theor. Phys. 109 (2003) 631

[37] K. Iida and K. Sato, Astrophys. J. 477 (1997) 294

[38] T. Strohmayer, H. M. van Horn, S. Ogata, H. Iyetomi, and S. Ichimaru, Astrophys. J. 375 (1991) 679

[39] S. Ogata and S. Ichimaru, Phys. Rev. A 42 (1990) 4867

[40] H. Sotani, Phys. Lett. B 730 (2014) 166

[41] F. Douchin and P. Haensel, Astron. Astrophys. 380 (2001) 151

[42] B. L. Schumaker and K. S. Thorne, Mon. Not. R. Astron. Soc. 203 (1983) 457

[43] H. Sotani, K. Iida, and K. Oyamatsu, Phys. Rev. C 91 (2015) 015805

[44] D. Kobyakov and C. J. Pethick, arXiv:1502.02461

[45] D. Kobyakov and C. J. Pethick, Phys. Rev. Lett. 112 (2014) 112504